Submitted to the
XXI International Symposium on Lepton and Photon Interactions at High Energies
11-16 August 2003 Fermi National Accelerator Laboratory, Batavia, Illinois USA

Search for Lepton Flavor Violation in τ production by ep collisions at HERA

ZEUS Collaboration

Abstract

A search has been made for lepton-flavor-violating interactions of the type $e^+p \to \tau X$, with the ZEUS detector at the HERA ep collider, using an integrated luminosity of 65.5 pb^{-1}. The data were taken at center-of-mass energy, $\sqrt{s}$, of 318 GeV, corresponding to a positron energy of 27.5 GeV and proton energy of 920 GeV. No evidence was found for lepton-flavor violation and constraints were derived for leptoquarks (LQ) that could mediate such interactions. For LQ masses below $\sqrt{s}$ limits were set on $\lambda_{eq_1}\sqrt{\beta_{\tau q}}$, where λ_{eq_1} is the coupling of the LQ to an electron and a first generation quark q_1 and $\beta_{\tau q}$ is the branching ratio of the LQ to τ and a quark q. For LQ masses exceeding $\sqrt{s}$, limits were set on the four-fermion interaction term $\lambda_{eq_\alpha}\lambda_{\tau q_\beta}/M_{LQ}^2$ for LQs that couple to an electron and a quark q_α and to a τ and a quark q_β. Some of the limits are also applicable to lepton-flavor-violating processes mediated by squarks in R-parity-violating supersymmetric models.

1 Introduction

In the Standard Model (SM) framework, lepton flavor is conserved. Minimal extensions to the SM [1] that allow for finite neutrino masses and, thereby, account for the observed neutrino oscillations [2,3] do not predict detectable rates of lepton-flavor-violation (LFV) in the charged lepton sector at current collider experiments. However, many other extensions of the SM, such as grand unified theories [4], models based on supersymmetry [5], compositeness [6] or technicolor [7] involve LFV interactions at detectable levels.

In high-energy e^+p collisions at HERA, reactions of the type $eq_i \to \tau q_f$, where q_i and q_f denote initial- and final-state quarks, the τ is expected to have a large transverse momentum and can be detected with high efficiency and small background. Such reactions, shown in Fig. 1 in case of a positron beam, can be mediated by leptoquarks (LQs), bosons that carry both lepton (L) and baryon (B) numbers and have lepton-quark Yukawa couplings. Such bosons arise naturally in unified theories that arrange quarks and leptons in common multiplets. Any LQ that couples leptons of two generations to each other would induce LFV. In this paper the Buchmüller-Rückl-Wyler (BRW) model [8] was used in order to classify LQ species and to evaluate cross sections of the LQ–induced processes. These processes can also be mediated by squarks in R–parity–violating SUSY models. Further details on these models and on the cross–section approximation used can be found elsewhere [9]. There are strong constraints from low energy experiments [10–13] on some of LFV processes, however HERA has an unique discovery potential for some cases where high generation of quarks are involved.

Previous searches for lepton-flavor-violation at HERA have been reported by ZEUS [9, 14–16] and H1 [17]. This paper reports on a search for LFV processes $e^+p \to \tau X$ using data collected by the ZEUS experiment in 1999 and 2000 at a center–of–mass energy, $\sqrt{s}$, of 318 GeV with an integrated luminosity of 65.5 pb^{-1}.

2 Event selection

Events from the reaction $e^+p \to \tau^+ X$, for example those mediated by a heavy LQ, are characterized by a high-transverse-momentum isolated τ balanced by a jet in the transverse plane. Since the τ decays close to the interaction vertex (in $\sim 65\%$ of the cases into hadrons and one neutrino and in $\sim 35\%$ into a charged lepton and two neutrinos), only its decay products are visible in the detector. Due to the presence of at least one neutrino in the final state, these events are characterized by a high value of the tranverse momentum imbalance, $\not{P}_t$, measured by the calorimeter. A detailed description of the ZEUS detector can be found elsewhere [18]. The main components used for this analysis are the central tracking detector (CTD) [19], the uranium calorimeter (CAL) [20], the forward muon detector (FMUON) [18] and the luminosity monitor [21,22]. Global calorimeter quantities, used in the event selection, were calculated as follows: to each calorimeter cell i with an energy deposit E_i above a threshold (80 MeV for electromagnetic calorimeter cells and 140 MeV for hadronic calorimeter cells) was assigned a four-momentum P^μ, defined as $P^\mu = (E_i, E_i \cos\phi_i \sin\theta_i, E_i \sin\phi_i \sin\theta_i, E_i \cos\theta_i)$, where ϕ_i and θ_i are the azimuthal and polar angles of the cell center relative to the event vertex[1]. The total momentum four-vector seen by the calorimeter (E, P_X, P_Y, P_Z) is given by the sum of the four-momenta for all cells. The transverse energy, E_t, is given by $\sum_i E_i \sin\theta_i$. The missing transverse momentum, $\not{P}_t$, is given by $\sqrt{P_X^2 + P_Y^2}$. The azimuthal angle assigned to $\not{P}_t$, $\phi_{\rm miss}$, was defined by $\cos\phi_{\rm miss} = -P_X/\not{P}_t$ and $\sin\phi_{\rm miss} = -P_Y/\not{P}_t$.

2.1 Trigger and preselection

The trigger, which is identical to that used in the charged current (CC) deep inelastic scattering (DIS) measurement described elsewhere [23], was based on a cut on $\not{P}_t$ with a considerably lower threshold than the selection cuts described below. After applying cuts to reject non-e^+p backgrounds (mainly cosmic rays and beam-gas interactions), the following pre-selection requirements were imposed:

- a reconstructed vertex with Z coordinate $|Z_{\rm VTX}| < 50\,{\rm cm}$;
- $\not{P}_t > 12\,{\rm GeV}$.

For each of the three possible decay channels of tau (hadrons ν_{tau}, $e\nu_\tau\nu_e$, $\mu\nu_\tau\nu_\mu$) dedicate final selection cuts, described in the following sections, are applied.

2.2 Hadronic τ decays

The following cuts were applied for the preselection of the hadronic tau decays:

- No electron with energy larger than 10 GeV;
- $E_t > 50\,{\rm GeV}$;
- $15 < E - P_z < 60\,{\rm GeV}$;
- a τ jet candidate (described below).

[1] The ZEUS coordinate system is a right-handed Cartesian system, with the Z axis pointing in the proton beam direction, referred to as the "forward direction", and the X axis pointing left towards the center of HERA. The coordinate origin is at the nominal interaction point.

The τ jet candidate was required to have a transverse momentum greater than 15 GeV, to be within the CTD acceptance ($15^\circ < \theta < 164^\circ$) and to have between one and three tracks pointing to the calorimeter deposition associated with the jet. In order to reject electrons from NC events a cut of 0.95 was applied on the electromagnetic energy fraction of the jet ($fEMC$). In addition the jet was requested to satisfy the condition $ltf + fEMC < 1.6$, where ltf (the leading track fraction) was defined as the ratio between the momentum of the most energetic track in the jet and the jet energy. In addition, a tau discriminant, D, was employed to separate tau from quark or gluon induced jets. This technique, based on the analysis of the jet shape, is described in Appendix A. Figures 2 and 3 show the comparison between data and MC for the jet variables and the discriminant, respectively. After the hadronic preselection 76 events were found in data, while 59 ± 8 were expected from SM processes, mainly from CC DIS.

For the final selection the following further cuts were applied:

- the τ jet candidate was required to be aligned in azimuth, ϕ, with the direction of the $\not{P}_t$ ($|\Delta\phi| < 20^\circ$),
- D > 0.9.

2.3 Leptonic τ decays

For the electron channel $\tau \to e\nu_\tau\bar{\nu}_e$, after the common preselection, the following selection criteria were required:

- $\not{P}_t > 15\,\mathrm{GeV}$;
- $20 < E - P_z < 52\,\mathrm{GeV}$;
- no energy deposit in the Rear Calorimeter (RCAL) larger than 7 GeV;
- $\not{P}_t/\sqrt{E_t} > 2.5\sqrt{\mathrm{GeV}}$;
- an electron with energy greater than 20 GeV in the polar angle region $8^\circ < \theta < 125^\circ$ and in the $\not{P}_t$ direction ($|\Delta\phi| < 20^\circ$).

In the muon decay channel $\tau \to \mu\nu_\tau\bar{\nu}_\mu$, an isolated muon in the $\not{P}_t$ direction was required. Forward muons ($8^\circ < \theta_\mu < 20^\circ$) were identified by a reconstructed track in FMUON, while central muons ($15^\circ < \theta_\mu < 164^\circ$) were found by performing a matching between a CTD track and calorimeter energy deposits consistent with those expected from a minimum ionizing particle. Since the muon contributes further to the $\not{P}_t$ in the calorimeter, the $\not{P}_t$ related cuts were enhanced ($\not{P}_t > 20\,\mathrm{GeV}$ and $\not{P}_t/\sqrt{E_t} > 3\sqrt{\mathrm{GeV}}$). The muon channel selection criteria are described in detail in [16].

3 Results

No candidate was found in the data from any of the three channels, while 0.8 ± 0.3 events were expected from SM processes, mainly CC DIS, di-muon and di-tau production in $\gamma\gamma$ interaction and photoproduction. The selection efficiencies were evaluated using signal MC events generated by LQGENEP [24]. For resonant production of lepton-flavor-violating scalar LQs, the selection efficiency varies from 24% to 30% for M_{LQ} from 140 GeV to 300 GeV, while the efficiency for vector LQs is in the range 25% to 37%. For LQs with $M_{\mathrm{LQ}} \gg \sqrt{s}$, the efficiencies are almost independent of M_{LQ}, but depend strongly on the generation of the quarks involved in the process. The selection efficiency ranges from 21% to 6.6% for $F = 0$ [2] LQs and from 20% to 6.2% for $|F| = 2$ LQs. In case the initial-state quark be a sea-quark, the efficiency is considerably lower, due to the softer quark x-spectrum causing lower transverse momenta for the final-state τ leptons.

Since no candidate was found, limits at 95% confidence level C.L. were set on the LFV process $e^+p \to \tau X$.

3.1 Low-mass LQ and squark limits

LQs with mass less than $\sqrt{s}$ are predominantly produced as narrow resonances in the s-channel. Limits at the 95% C.L. on $\lambda_{eq_1}\sqrt{\beta_{\tau q}}$ (where λ_{eq_1} is the coupling of the LQ to an electron and a first generation quark q_1 and $\beta_{\tau q}$ is the branching ratio of the LQ to τ and a quark q) were derived for F=0 LQs. The limits were obtained using the narrow–width approximation for the cross section corrected for QED initial-state radiation (ISR) and next-to-leading-order QCD effects [25, 26] (only for scalar LQs). These limits apply to processes involving any quark generation in the final state (excluding the $t-$quark). Figures 4(a-b) show the upper limits on $\lambda_{eq_1}\sqrt{\beta_{\tau q}}$ for scalar and vector LQs, respectively. Under the assumption that $\lambda_{eq_1} = \lambda_{\tau q_\beta}$, limits on λ_{eq_1} can be derived. These are compared to limits, which are generation specific, from low-energy experiments in Figs. 4(c-d) for $\tilde{S}^L_{1/2}$ and V^R_0 LQs. Since these states do not couple to neutrinos, $\beta_{\tau q} = \beta_{eq} = 0.5$ is assumed. The limits on $\lambda_{eq_1}\sqrt{\beta_{\tau q}}$ for $\tilde{S}^L_{1/2}$ can be interpreted as limits on $\lambda'_{1j1}\sqrt{\beta_{\tilde{u}^j\to\tau q}}$ for $\tilde{u}^j$ squarks of generation j, where λ'_{1j1} is the coupling constant for the process $e^+d \to \tilde{u}^j$ and $\beta_{\tilde{u}^j\to\tau q}$ is the branching ratio of $\tilde{u}^j$ in τq.

Another way to illustrate the sensitivity of the search is to assume that the couplings have electromagnetic strength ($\lambda_{eq_1} = \lambda_{\tau q_\beta} = 0.3 \approx \sqrt{4\pi\alpha}$). In this case, LQs with masses up to 299 GeV are excluded, as shown in Table 1. Alternatively, as shown in Table 2, for a fixed M_{LQ} of 250 GeV, values of $\lambda_{eq_1}\sqrt{\beta_{\tau q}}$ down to 0.013 are excluded.

[2] $F = 3B + L$ is the LQ fermionic number, B and L being the baryon and lepton number, respectively

3.2 High-mass LQ and squark limits

For leptoquarks with mass much greater than $\sqrt{s}$, the cross-section limit provides a direct limit on $\lambda_{eq_\alpha}\lambda_{\tau q_\beta}/M_{\rm LQ}^2$ ($M_{\rm LQ}$ is the LQ mass, α and β denote the quark generations) using the contact–interaction approximation with QED-ISR corrections. The CTEQ5 [27] parametrizations of parton densities were used to evaluate cross sections. Tables 3 and 4 show the limits for $F = 0$ and $|F| = 2$ LQs, respectively, calculated for all combination of quark generation (α, β) coupling to the LQs.

In many cases involving c and b quarks, the ZEUS limits improve existing low-energy limits [10–13]. Results obtained by H1 [17] are comparable to ZEUS results.

The limits on $\lambda_{eq_\alpha}\lambda_{\tau q_\beta}/M_{\rm LQ}^2$ for $\tilde{S}^L_{1/2}$ can be interpreted as limits on $\lambda'_{1j\alpha}\lambda'_{2j\beta}/M^2_{\tilde{u}}$ for a u-type squark of generation j. Similarly, the limits on S_0^L LQs can be interpreted as limits on $\lambda'_{1\alpha k}\lambda'_{2\beta k}/M^2_{\tilde{d}}$ for a d-type squark of generation k.

4 Conclusions

A search for lepton-flavor violation was performed using an integrated luminosity of $65.5\,\text{pb}^{-1}$ of e^+p data at $\sqrt{s} = 318\,\text{GeV}$ collected with the ZEUS detector at HERA in 1999–2000. No evidence for LFV processes was found.

Limits at 95% C.L. on couplings and masses for F=0 leptoquarks that mediate LFV processes were set. Assuming the couplings $\lambda_{eq_1} = \lambda_{\tau q_\beta} = 0.3$, lower mass limits between 276 and 299 GeV were derived for various LQs decaying to τq. For $M_{\rm LQ} = 250\,\text{GeV}$, upper limits for $\lambda_{eq_1}\sqrt{\beta_{\tau q}}$ in the range $(1.3-6.5)\cdot 10^{-2}$ were obtained. Limits on $\tilde{S}^L_{1/2}$ also apply to up-type squarks that have R-parity-violating couplings to a positron and a τ.

For LQs with $M_{\rm LQ} \gg \sqrt{s}$, upper limits on $\lambda_{eq_\alpha}\lambda_{\tau q_\beta}/M_{\rm LQ}^2$ were obtained and compared with bounds from low-energy experiments. Some of these limits also apply to high-mass R_p-violating squarks. In many cases, particularly when higher-generation quarks are involved, the ZEUS limits are the most stringent.

A Tau identification

The hadronic tau decays are characterized by a "pencil like" jet with a low charged-multiplicity of tracks detected in the CTD. It is possible, thus, to distinguish tau jets from quark and gluon induced jets, using jet variables [28]. The jet definition was based on the longitudinally invariant k_T cluster algorithm [29]. Lepton flavor violating MC events generated with LQGENEP, with the final state τ decaying into hadrons and neutrino, were used to simulate the signal. The background simulation was based on CC DIS events using the generator DJANGO6 [30], an interface to the programs HERACLES 4.5 [31] and LEPTO 6.4 [32]. The jet shape was characterized by six observables: the first ($\mathrm{R_{mean}}$) and the second ($\mathrm{R_{rms}}$) moment of the radial extension of the jet energy deposition; the first ($\mathrm{L_{mean}}$) and the second ($\mathrm{L_{rms}}$) moment of the energy deposition in the direction along the jet axis; the number of subjets ($\mathrm{N_{subj}}$) with a y_{cut} of $5 \cdot 10^{-4}$ [33, 34]; the mass ($\mathrm{M_{jet}}$) of the jet calculated from the calorimeter cells associated to the jet. For a detailed definition of these variables see [35]. In Fig. 2 the distribution of the six jet variables for the data, the signal MC and the background MC (mainly charged current DIS, neutral current DIS and direct and resolved photoproduction) after the hadronic preselection are shown. In order to separate the signal from the background, the six variables were combined in a discriminant D, given, from any point in the phase space $\vec{x}(-\log(\mathrm{R_{mean}}), -\log(\mathrm{R_{rms}}), -\log(1-\mathrm{L_{mean}}), -\log(\mathrm{L_{rms}}), \mathrm{N_{subj}}, \mathrm{M_{jet}})$, as:

$$\mathrm{D}(\vec{x}) = \frac{\rho_{sig}(\vec{x})}{\rho_{sig}(\vec{x}) + \rho_{bg}(\vec{x})},$$

where ρ_{sig} and ρ_{bg} are the density functions of the signal and the background, respectively. The densities, sampled using MC simulations, were calculated using a method which is based on range searching (PDE-RS) [36]. For any given jet with phase space coordinates $\vec{x}$, the signal and the background densities are evaluated from the number of corresponding signal and background jets in a 6-dimensional box of fixed size, which is centered around $\vec{x}$. The tau signal tends to have a large discriminant value ($\mathrm{D} \rightarrow 1$) while the CC DIS background has a low discriminant value ($\mathrm{D} \rightarrow 0$) as can be seen in Fig. 3.

References

[1] Z. Maki, M. Nakagawa and S. Sakata, Prog. Theor. Phys. **28**, 870 (1962); P. Fisher, B. Kayser and K.S. McFarland, Ann. Rev. Nucl. Part. Sci. **49**, 481 (1999).

[2] Super-Kamiokande Coll., Y. Fukuda et al., Phys. Rev. Lett. **81**, 1562 (1998).

[3] SNO Coll., Q.R. Ahmad et al., Phys. Rev. Lett. **87**, 071301 (2001).

[4] J.C. Pati and A. Salam, Phys. Rev. **D 10**, 275 (1974); H. Georgi and S.L. Glashow, Phys. Rev. Lett. **32**, 438 (1974); P. Langacker, Phys. Rep. **72**, 185 (1981).

[5] H.P. Nilles, Phys. Rep. **110**, 1 (1984); H.E. Haber and G.L. Kane, Phys. Rep. **117**, 75 (1985).

[6] B. Schrempp and F. Schrempp, Phys. Lett. **B 153**, 101 (1985); J. Wudka, Phys. Lett. **B 167**, 337 (1986).

[7] S. Dimopoulos and L. Susskind, Nucl. Phys. **B 155**, 237 (1979); S. Dimopoulos, Nucl. Phys. **B 168**, 69 (1980); E. Farhi and L. Susskind, Phys. Rev. **D 20**, 3404 (1979); E. Farhi and L. Susskind, Phys. Rep. **74**, 277 (1981).

[8] W. Buchmüller, R. Rückl and D. Wyler, Phys. Lett. **B 191**, 442 (1987). Erratum in Phys. Lett. **B 448**, 320 (1999).

[9] ZEUS Coll., S. Chekanov et al., Phys. Rev. **D 65**, 92004 (2002).

[10] S. Davidson, D. Bailey and B.A. Campbell, Z. Phys. **C 61**, 613 (1994).

[11] Herz, Margarete, *Bounds on leptoquark and supersymmetric, R-parity violating interactions from meson decays. (In German).* Thesis, Report hep-ph/0301079, 2002.

[12] E. Gabrielli, Phys. Rev. **D 62**, 055009 (2000).

[13] Particle Data Group, K. Hagiwara et al., Phys. Rev. **D 66**, 10001 (2002).

[14] ZEUS Coll., M. Derrick et al., Z. Phys. **C 73**, 613 (1997).

[15] ZEUS Coll., *Search for lepton-flavor violation in ep collisions at HERA.* Paper 605 submitted to the International Europhysics Conference on High Energy Physics 01, Budapest, Hungary, July 12-18 2001, 2001.

[16] ZEUS Coll., *Search for lepton-flavor violation in ep collision at HERA.* Abstract 906, 31st International Conference on High Energy Physics, Amsterdam, Netherlands, 2002, 2002.

[17] H1 Coll., C. Adloff et al., Eur. Phys. J. **C 11**, 447 (1999). Erratum in Eur. Phys. J. C14, 553 (2000).

[18] ZEUS Coll., U. Holm (ed.), *The ZEUS Detector*. Status Report (unpublished), DESY (1993), available on `http://www-zeus.desy.de/bluebook/bluebook.html`.

[19] N. Harnew et al., Nucl. Inst. Meth. **A 279**, 290 (1989);
B. Foster et al., Nucl. Phys. Proc. Suppl. **B 32**, 181 (1993);
B. Foster et al., Nucl. Inst. Meth. **A 338**, 254 (1994).

[20] M. Derrick et al., Nucl. Inst. Meth. **A 309**, 77 (1991);
A. Andresen et al., Nucl. Inst. Meth. **A 309**, 101 (1991);
A. Caldwell et al., Nucl. Inst. Meth. **A 321**, 356 (1992);
A. Bernstein et al., Nucl. Inst. Meth. **A 336**, 23 (1993).

[21] J. Andruszków et al., Preprint DESY-92-066, DESY, 1992;
ZEUS Coll., M. Derrick et al., Z. Phys. **C 63**, 391 (1994).

[22] J. Andruszków et al., Acta Phys. Pol. **B 32**, 2025 (2001).

[23] ZEUS Coll., J. Breitweg et al., Eur. Phys. J. **C 12**, 411 (2000).

[24] L. Bellagamba, Comp. Phys. Comm. **141**, 83 (2001).

[25] T. Plehn et al., Z. Phys. **C 74**, 611 (1997).

[26] Z. Kunszt and W.J. Stirling, Z. Phys. **C 75**, 453 (1997).

[27] CTEQ Coll., H.L. Lai et al., Eur. Phys. J. **C 12**, 375 (2000).

[28] C.N. Nguyen. Diploma Thesis, Universität Hamburg, Hamburg, Germany, Report DESY-THESIS-2002-024, 2002.

[29] S.Catani et al., Nucl. Phys. **B406**, 187 (1993);
S.D. Ellis and D.E. Soper, Phys. Rev. **D 48**, 3160 (1993);
M. H. Seymour, Nucl. Phys. **B513**, 269 (1998).

[30] K. Charchula, G.A. Schuler and H. Spiesberger, Comp. Phys. Comm. **81**, 381 (1994).

[31] A. Kwiatkowski, H. Spiesberger and H.-J. Möhring, Comp. Phys. Comm. **69**, 155 (1992). Also in *Proc. Workshop Physics at HERA*, 1991, DESY, Hamburg.

[32] G. Ingelman, A. Edin and J. Rathsman, Comp. Phys. Comm. **101**, 108 (1997).

[33] J. R. Forshaw and M. H. Seymour, JHEP **09**, 009 (1999).

[34] M. H. Seymour, Nucl. Phys. **B421**, 545 (1994).

[35] ZEUS Coll., *Search for events with isolated tau leptons and large missing transverse momentum in ep collisions at HERA*. Abstract 909, 31st International Conference on High Energy Physics, Amsterdam, Netherlands, 2002, 2002.

[36] T. Carli and B. Koblitz. Batavia, USA, 2000, Adv. Comp. Analysis Techniques in Phys. Research P. Bath and M. Kasemann, Eds., pp 110, also in hep-ph/0011224, 2000;
T. Carli and B. Koblitz, Nucl. Inst. Meth. **A501**, 576 (2003).

LQ type	$\tilde{S}^L_{1/2}$	$S^L_{1/2}$	$S^R_{1/2}$	V^L_0	V^R_0	$\tilde{V}^R_0$	V^L_1
τ-channel limit on $M_{\mathrm{LQ}}(\,\mathrm{GeV})$	276	293	293	276	281	296	299

Table 1: *The* 95% *C.L. lower limits on* M_{LQ} *assuming* $\lambda_{eq_1} = \lambda_{\tau q} = 0.3$.

LQ type	$\tilde{S}^L_{1/2}$	$S^L_{1/2}$	$S^R_{1/2}$	V^L_0/V^R_0	$\tilde{V}^R_0$	V^L_1
τ-channel limit on $\lambda_{eq_1}\sqrt{\beta_{\tau q}}$	0.065	0.028	0.026	0.045	0.020	0.013

Table 2: *The* 95% *C.L. upper limits on* $\lambda_{eq_1}\sqrt{\beta_{\tau q}}$ *for a leptoquark with mass* $M_{\mathrm{LQ}} = 250\ GeV$.

$e \to \tau$			ZEUS		$F = 0$		
$\boldsymbol{\alpha\beta}$	$\boldsymbol{S^L_{1/2}}$ e^+u_α	$\boldsymbol{S^R_{1/2}}$ $e^+(u+d)_\alpha$	$\boldsymbol{\tilde{S}^L_{1/2}}$ e^+d_α	$\boldsymbol{V^L_0}$ e^+d_α	$\boldsymbol{V^R_0}$ e^+d_α	$\boldsymbol{\tilde{V}^R_0}$ e^+u_α	$\boldsymbol{V^L_1}$ $e^+(\sqrt{2}u+d)_\alpha$
1 1	$\tau \to \pi e$ 0.4 **2.2**	$\tau \to \pi e$ 0.2 **1.8**	$\tau \to \pi e$ 0.4 **3.2**	$\tau \to \pi e$ 0.2 **2.3**	$\tau \to \pi e$ 0.2 **2.3**	$\tau \to \pi e$ 0.2 **1.7**	$\tau \to \pi e$ 0.06 **0.8**
1 2	$\boxed{\mathbf{2.2}}$	$\tau \to Ke$ 6.3 $\boxed{\mathbf{1.9}}$	$K \to \pi\nu\bar{\nu}$ 5.8×10^{-4} **3.4**	$\tau \to Ke$ 3.2 $\boxed{\mathbf{2.6}}$	$\tau \to Ke$ 3.2 $\boxed{\mathbf{2.6}}$	$\boxed{\mathbf{1.9}}$	$K \to \pi\nu\bar{\nu}$ 1.5×10^{-4} **0.9**
1 3	*	$B \to \tau\bar{e}$ 0.6 **3.8**	$B \to \tau\bar{e}$ 0.6 **3.8**	$B \to \tau\bar{e}$ 0.3 **3.2**	$B \to \tau\bar{e}$ 0.3 **3.2**	*	$B \to \tau\bar{e}$ 0.3 **3.2**
2 1	$\boxed{\mathbf{11}}$	$\tau \to Ke$ 6.3 **6.4**	$K \to \pi\nu\bar{\nu}$ 5.8×10^{-4} **7.8**	$\tau \to Ke$ 3.2 **3.5**	$\tau \to Ke$ 3.2 **3.5**	$\boxed{\mathbf{4.6}}$	$K \to \pi\nu\bar{\nu}$ 1.5×10^{-4} **1.9**
2 2	$\tau \to ee\bar{e}$ 20 $\boxed{\mathbf{13}}$	$\tau \to ee\bar{e}$ 30 $\boxed{\mathbf{7.3}}$	$\tau \to ee\bar{e}$ 66 $\boxed{\mathbf{8.9}}$	$\tau \to ee\bar{e}$ 33 $\boxed{\mathbf{4.4}}$	$\tau \to ee\bar{e}$ 33 $\boxed{\mathbf{4.4}}$	$\tau \to ee\bar{e}$ 10 $\boxed{\mathbf{7.1}}$	$\tau \to ee\bar{e}$ 6.1 $\boxed{\mathbf{2.7}}$
2 3	*	$B \to \tau\bar{e}X$ 14 $\boxed{\mathbf{11}}$	$B \to \tau\bar{e}X$ 14 $\boxed{\mathbf{11}}$	$B \to \tau\bar{e}X$ 7.2 $\boxed{\mathbf{6.8}}$	$B \to \tau\bar{e}X$ 7.2 $\boxed{\mathbf{6.8}}$	*	$B \to \tau\bar{e}X$ 7.2 $\boxed{\mathbf{6.8}}$
3 1	*	$B \to \tau\bar{e}$ 0.6 **11**	$B \to \tau\bar{e}$ 0.6 **11**	V_{ub} 0.12 **4.0**	$B \to \tau\bar{e}$ 0.3 **4.0**	*	V_{ub} 0.12 **4.0**
3 2	*	$B \to \tau\bar{e}X$ 14 **14**	$B \to \tau\bar{e}X$ 14 **14**	$B \to \tau\bar{e}X$ 7.2 $\boxed{\mathbf{5.2}}$	$B \to \tau\bar{e}X$ 7.2 $\boxed{\mathbf{5.2}}$	*	$B \to \tau\bar{e}X$ 7.2 $\boxed{\mathbf{5.2}}$
3 3	*	$\tau \to ee\bar{e}$ 30 $\boxed{\mathbf{19}}$	$\tau \to ee\bar{e}$ 66 $\boxed{\mathbf{19}}$	$\tau \to ee\bar{e}$ 33 $\boxed{\mathbf{10}}$	$\tau \to ee\bar{e}$ 33 $\boxed{\mathbf{10}}$	*	$\tau \to ee\bar{e}$ 6.1 **10**

Table 3: *Upper limits at 95% C.L. on $\lambda_{eq_\alpha}\lambda_{\tau q_\beta}/M^2_{LQ}$ in units of* TeV^{-2}*, for $F = 0$ LQs that couple to eq_α and to τq_β. The columns correspond to the $F = 0$ LQ species. The eq_α combination for e^+p collisions and s-channel case is reported under the LQ type (the combination for e^-p collisions can be obtained by applying charge conjugation). Each row corresponds to a different combination of quark generations (α, β) that couple to the e and the τ, respectively. Within each cell, the measurement that provides the most stringent low–energy constraint is shown on the first line and the corresponding limit [10–13] is given on the second line. The ZEUS limits are shown on the third line of each cell (enclosed in a box when stronger than the low–energy constraint). The * indicates cases where a top quark must be involved.*

$e \to \tau$ ZEUS $\lvert F \rvert = 2$							
$\boldsymbol{\alpha\beta}$	$\boldsymbol{S_0^L}$ $e^+\bar{u}_\alpha$	$\boldsymbol{S_0^R}$ $e^+\bar{u}_\alpha$	$\boldsymbol{\tilde{S}_0^R}$ $e^+\bar{d}_\alpha$	$\boldsymbol{S_1^L}$ $e^+(\bar{u}+\sqrt{2}\bar{d})_\alpha$	$\boldsymbol{V_{1/2}^L}$ $e^+\bar{d}_\alpha$	$\boldsymbol{V_{1/2}^R}$ $e^+(\bar{u}+\bar{d})_\alpha$	$\boldsymbol{\tilde{V}_{1/2}^L}$ $e^+\bar{u}_\alpha$
1 1	$\boldsymbol{G_F}$ 0.3 **3.8**	$\boldsymbol{\tau \to \pi e}$ 0.4 **3.8**	$\boldsymbol{\tau \to \pi e}$ 0.4 **4.9**	$\boldsymbol{\tau \to \pi e}$ 0.1 **2.1**	$\boldsymbol{\tau \to \pi e}$ 0.2 **1.8**	$\boldsymbol{\tau \to \pi e}$ 0.1 **1.0**	$\boldsymbol{\tau \to \pi e}$ 0.2 **1.2**
1 2	$\boldsymbol{K \to \pi\nu\bar{\nu}}$ 5.8×10^{-4} **8.6**	$\boxed{\mathbf{8.6}}$	$\boldsymbol{\tau \to Ke}$ 6.3 **6.5**	$\boldsymbol{K \to \pi\nu\bar{\nu}}$ 2.9×10^{-4} **3.1**	$\boldsymbol{K \to \pi\nu\bar{\nu}}$ 2.9×10^{-4} **4.0**	$\boldsymbol{\tau \to Ke}$ 3.2 **3.2**	$\boxed{\mathbf{5.6}}$
1 3	$\boldsymbol{V_{ub}}$ 0.24 *	*	$\boldsymbol{B \to \tau\bar{e}}$ 0.6 **7.6**	$\boldsymbol{V_{ub}}$ 0.12 **3.8**	$\boldsymbol{B \to \tau\bar{e}}$ 0.3 **5.7**	$\boldsymbol{B \to \tau\bar{e}}$ 0.3 **5.7**	*
2 1	$\boldsymbol{K \to \pi\nu\bar{\nu}}$ 5.8×10^{-4} **4.1**	$\boxed{\mathbf{4.1}}$	$\boldsymbol{\tau \to Ke}$ 6.3 $\boxed{\mathbf{5.1}}$	$\boldsymbol{K \to \pi\nu\bar{\nu}}$ 2.9×10^{-4} **2.2**	$\boldsymbol{K \to \pi\nu\bar{\nu}}$ 2.9×10^{-4} **1.9**	$\boldsymbol{\tau \to Ke}$ 3.2 $\boxed{\mathbf{1.1}}$	$\boxed{\mathbf{1.3}}$
2 2	$\boldsymbol{\tau \to ee\bar{e}}$ 20 $\boxed{\mathbf{13}}$	$\boldsymbol{\tau \to ee\bar{e}}$ 20 $\boxed{\mathbf{13}}$	$\boldsymbol{\tau \to ee\bar{e}}$ 66 $\boxed{\mathbf{8.8}}$	$\boldsymbol{\tau \to ee\bar{e}}$ 55 $\boxed{\mathbf{4.1}}$	$\boldsymbol{\tau \to ee\bar{e}}$ 33 $\boxed{\mathbf{4.5}}$	$\boldsymbol{\tau \to ee\bar{e}}$ 15 $\boxed{\mathbf{3.8}}$	$\boldsymbol{\tau \to ee\bar{e}}$ 10 $\boxed{\mathbf{7.1}}$
2 3	*	*	$\boldsymbol{B \to \tau\bar{e}X}$ 14 $\boxed{\mathbf{10}}$	$\boldsymbol{B \to \tau\bar{e}X}$ 7.2 $\boxed{\mathbf{5.2}}$	$\boldsymbol{B \to \tau\bar{e}X}$ 7.2 $\boxed{\mathbf{6.8}}$	$\boldsymbol{B \to \tau\bar{e}X}$ 7.2 $\boxed{\mathbf{6.8}}$	*
3 1	*	*	$\boldsymbol{B \to \tau\bar{e}}$ 0.6 **6.9**	$\boldsymbol{B \to \tau\bar{e}}$ 0.3 **3.4**	$\boldsymbol{B \to \tau\bar{e}}$ 0.3 **2.0**	$\boldsymbol{B \to \tau\bar{e}}$ 0.3 **2.0**	*
3 2	*	*	$\boldsymbol{B \to \tau\bar{e}X}$ 14 **14**	$\boldsymbol{B \to \tau\bar{e}X}$ 7.2 $\boxed{\mathbf{7.1}}$	$\boldsymbol{B \to \tau\bar{e}X}$ 7.2 $\boxed{\mathbf{5.5}}$	$\boldsymbol{B \to \tau\bar{e}X}$ 7.2 $\boxed{\mathbf{5.5}}$	*
3 3	*	*	$\boldsymbol{\tau \to ee\bar{e}}$ 66 $\boxed{\mathbf{20}}$	$\boldsymbol{\tau \to ee\bar{e}}$ 55 $\boxed{\mathbf{10}}$	$\boldsymbol{\tau \to ee\bar{e}}$ 33 $\boxed{\mathbf{10}}$	$\boldsymbol{\tau \to ee\bar{e}}$ 15 $\boxed{\mathbf{10}}$	*

Table 4: *Upper limits at 95% C.L. on* $\lambda_{eq_\alpha}\lambda_{\tau q_\beta}/M_{LQ}^2$ *in units of* TeV^{-2}*, for* $|F| = 2$ *LQs that couple to* eq_α *and to* τq_β*. The columns correspond to the* $|F| = 2$ *LQ species. The format of the table is described in the caption of Table 3.*

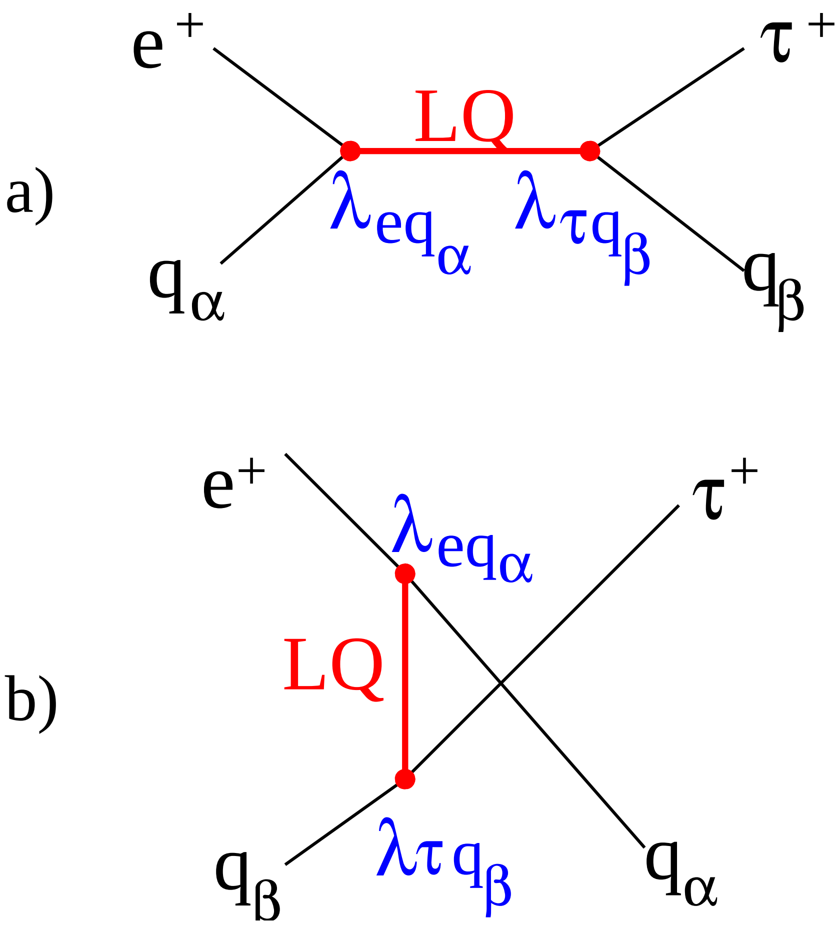

Figure 1: *(a) s-channel and (b) u-channel diagrams contributing to LFV processes induced by $F = 0$ LQs, where $F = 3B + L$ is the LQ fermionic number, B and L being baryon and lepton numbers, respectively. The subscripts α and β denote the quark generations. In e^+p scattering, $|F| = 2$ LQs couple to antiquarks in the s-channel and to quarks in the u-channel.*

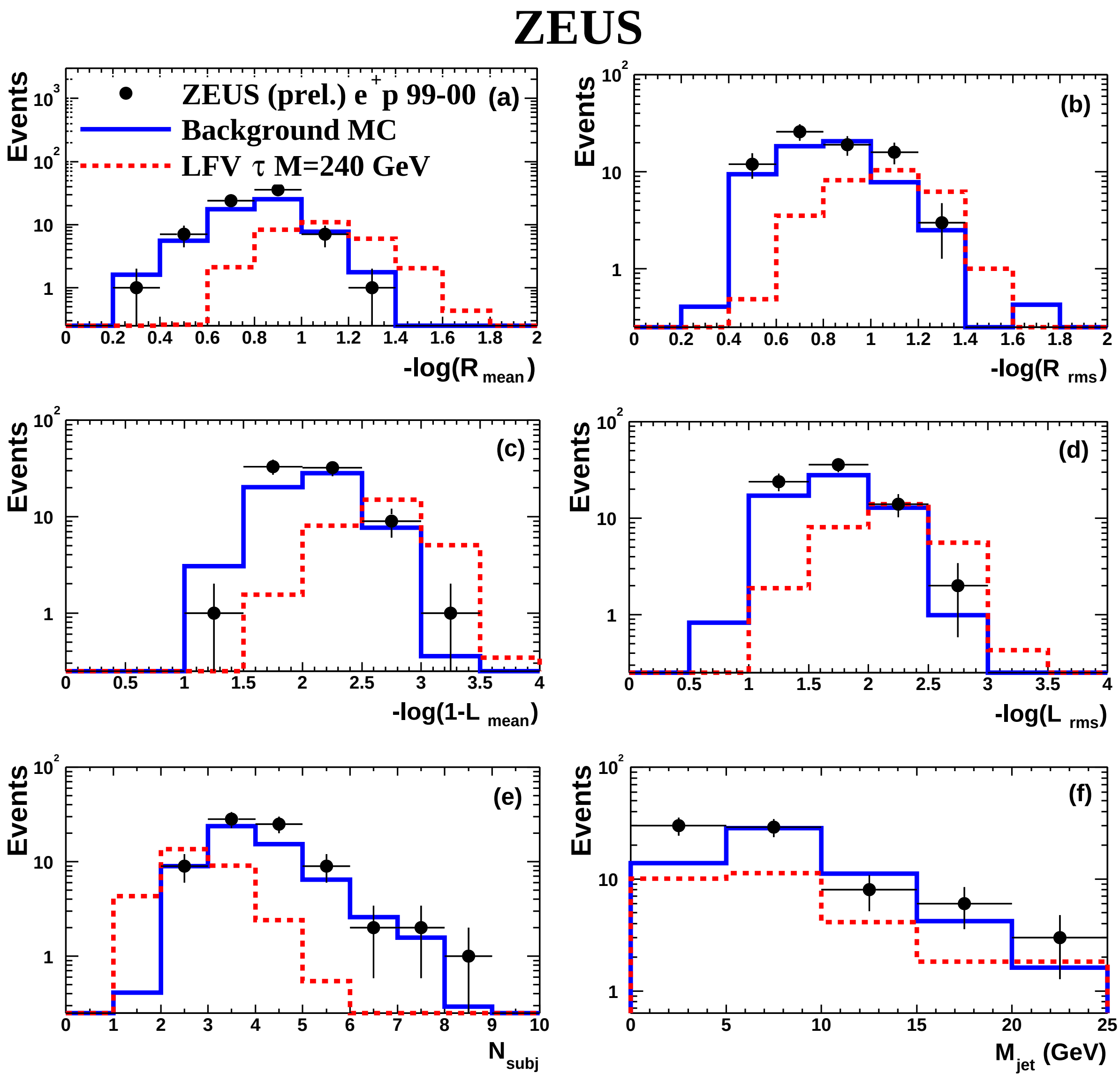

Figure 2: *Observables characterising the internal jet structure for data (solid points), SM simulation (solid line) and for the LFV signal (dotted line) after the hadronic preselection described in Sec. 2.2. The normalization for the signal is arbitrary. In each event only the jet with the highest value of the discriminant enters.*

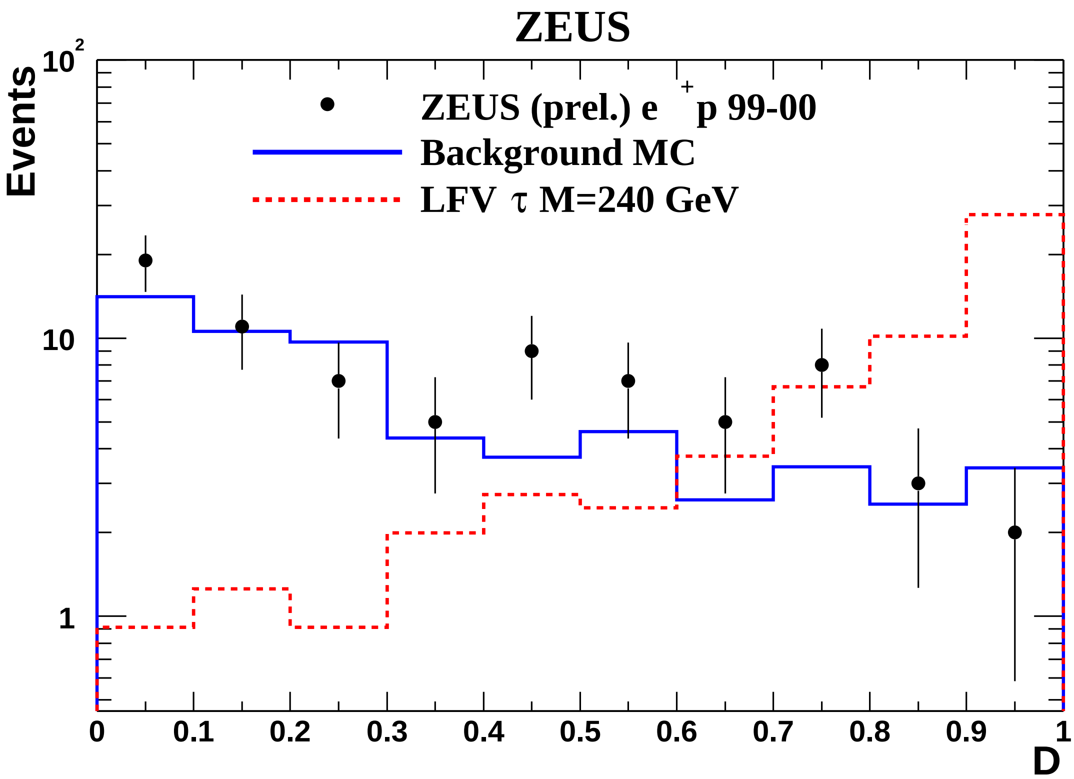

Figure 3: *Distribution of the tau discriminant for data (solid points), SM simulation (solid line) and for the LFV signal (dotted line) after the hadronic preselection described in Sec. 2.2. The normalization for the signal is arbitrary. In each event only the jet with the highest value of the discriminant enters.*

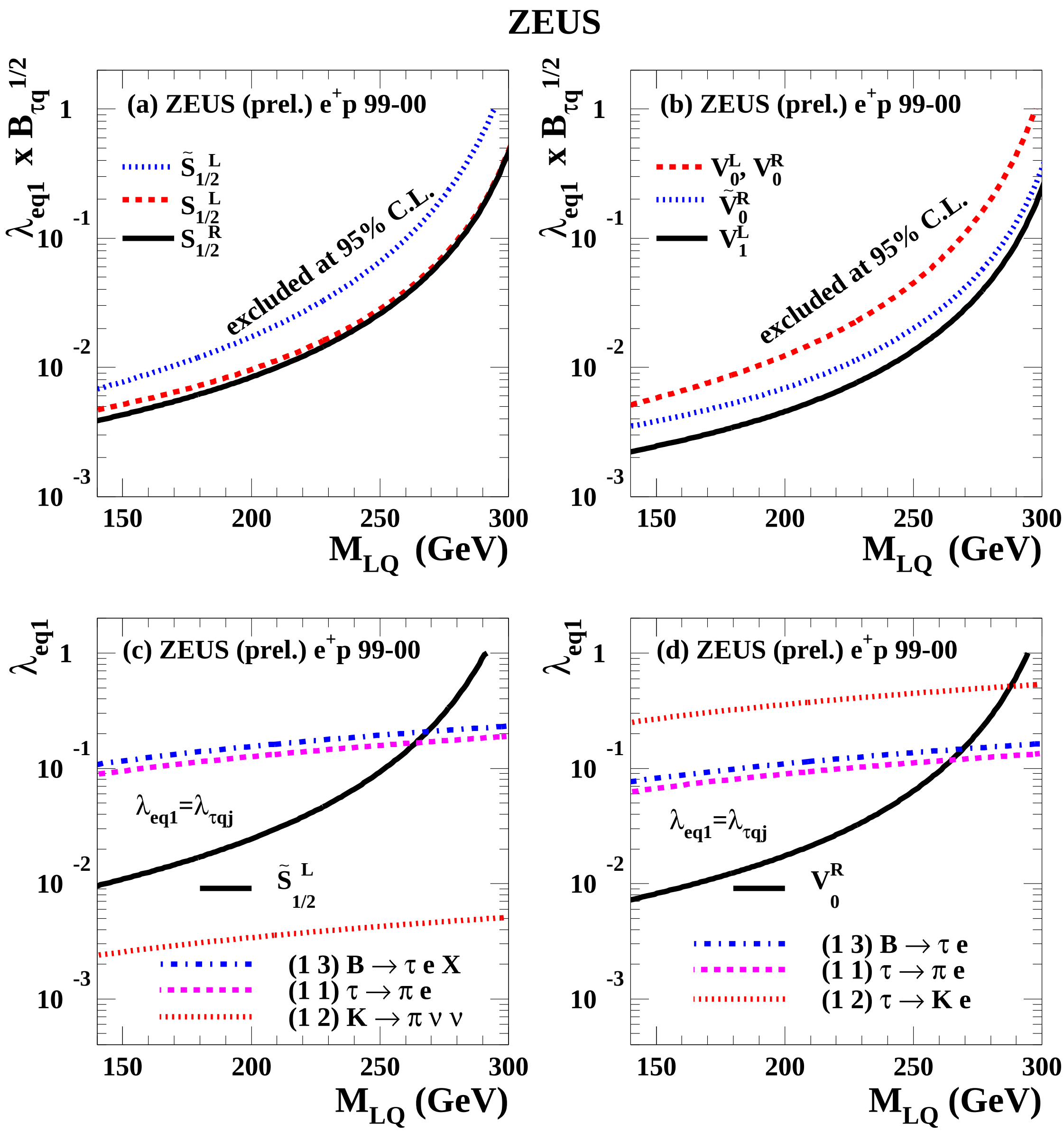

Figure 4: *Upper limits on* $\lambda_{eq_1}\sqrt{\beta_{\tau q}}$ *vs.* $M_{\rm LQ}$ *for lower mass (a) scalar and (b) vector LQs. Upper limits on* λ_{eq_1} *under the assumption* $\beta_{\tau q} = 0.5$ *are shown in (c) for scalar LQs and (d) for vector LQs that couple to d-type quarks. Also shown in (c) and (d) are existing limits [10–13] (dashed, dash-dotted and dotted lines). The numbers in parentheses indicate the generation numbers of the quarks that couple to the e and the* τ*, respectively. The regions above the curves are excluded at the 95% C.L.*